On the Feasibility of Millimeter-wave Backscatter using Commodity 802.11ad 60 GHz Radios

Yoon Chae
Department of Computer Science,
George Mason University
ychae2@gmu.edu

Parth Pathak
Department of Computer Science,
George Mason University
phpathak@gmu.edu

Kang Min Bae
Department of Electrical Engineering,
KAIST
bkm2259@kaist.ac.kr

Song Min Kim
Department of Electrical Engineering,
KAIST
songmin@kaist.ac.kr

ABSTRACT

Backscattering RFIDs have emerged as a versatile platform for low-power wireless networking and sensing in the era of Internet-of-Things (IoT). At the same time, millimeter-wave (mmWave) wireless has gained substantial attraction with high-speed WLAN and 5G cellular networks. Although the majority of RFID backscatter research focuses on lower frequencies, mmWave backscatter provides unique opportunities due to its directionality and wide bandwidth. Existing mmWave backscatter systems rely on expensive, custom-designed, dedicated readers which limit their widespread use. In this work, we present an empirical characterization of the first-of-its-kind mmWave backscatter system using 60 GHz commercial off-the-shelf (COTS) 802.11ad radios. Our presented system only relies on Channel State Information (CSI) and requires no modification to hardware or protocol. Through experimentation, we demonstrate that mmWave backscatter can be detected at a distance of up to $6m$ at different angles and locations. We also present how the backscatter can be leveraged in estimating the blockages in a WLAN which can reduce the beamsearching overhead. Our work opens a new direction of research where mmWave backscatter can be used to realize an integrated mmWave networking, sensing, and applications.

CCS CONCEPTS

• **Networks** → **Wireless local area networks**.

KEYWORDS

millimeter-wave, RFID backscatter, MMID, 802.11ad, 802.11ay, 60 GHz, Channel State Information (CSI)

1 INTRODUCTION

Backscatter radios and RFIDs have revolutionized the low-power and battery-less wireless networking in the past few years with applications in logistics, supply chain, healthcare, smart cities, human-computer interaction, tracking, sensing, etc. Majority of the backscatter and RFID communication currently target lower frequencies (900 MHz UHF or 2.4 GHz). The use of higher frequencies, especially the millimeter-wave (mmWave) spectrum, is leading the way in the development of the next generation of cellular (5G NR) and WLAN (802.11ad/ay) networks. With the availability of large unlicensed spectrum, backscatter communication at 60 GHz mmWave provides new opportunities.

Millimeter-wave backscatter and identification (mmID, analogous to RFID) provide several benefits over UHF RFID. First, with the use of directional communication and beamforming, it is possible to accurately locate mmID tags even when they are densely deployed, enabling novel applications such as item-level tagging. Tag localization at lower frequencies such as UHF is more challenging and requires either large/bulky directional antenna or antenna arrays [26, 29] for AoA/AoD estimation or multiple readers [15, 20]. Second, due to shorter wavelengths, mmIDs can use miniaturized high-gain patch array antennas resulting in a small form-factor. Hence, mmIDs can be easily embedded in size-restricted wearables and even implants for sensing applications. Third, with a large available bandwidth, gigabit backscatter communication is feasible with mmIDs. Gigabit backscatter can enable new applications such as short-range and high-speed bulk data retrieval from mmID (for example, quickly transferring a large file). Due to these advantages, mmIDs have been investigated in a few research works [11, 12, 17, 24, 25, 30] with the focus being on mmID tag design, and detection and localization of the mmID tags.

The objective of this work is to demonstrate the feasibility of mmWave backscatter using 60 GHz commercial off-the-shelf (COTS) 802.11ad devices. Specifically, we show that commodity 802.11ad devices such an AP can act as a mmWave backscatter reader by extracting the channel state information (CSI). There are numerous advantages of leveraging 802.11ad APs as mmID readers. First, it

will eliminate the need for special purpose mmID readers as commodity devices can be readily used to communicate with mmIDs. Second, 802.11ad and ay protocol frames can be retrofitted to read or write to (passive, semi-passive, or active) mmIDs making it possible to support communication between high-speed WLAN devices and low-power mmID tags. Third, the mmID tags can be seamlessly integrated into 802.11ad/ay WLANs which can enhance their ability to better understand the channel dynamics including mobility of clients and blockages. This information can then be used to improve the beam forming and steering efficiency as we show in this work.

In this work, we present a measurement-based characterization of mmWave backscatter using COTS 802.11ad devices. To the best of our knowledge, this is the first study to demonstrate the detection of mmWave backscatter using commodity 802.11ad devices without any hardware modifications. We use a state-of-the-art 802.11ad platform (from Airfide Inc. [3]) and extract CSI through driver modifications. We then analyze the CSI between two 802.11ad devices when the signal is backscattered from an mmWave tag. Since the development of a fast-switching mmWave tag is part of our ongoing work, we manually switch the mmWave antenna between open and short circuits to realize amplitude modulation on an mmID tag. Through the characterization, we make the following contributions: (1) We show that 802.11ad COTS devices can provide a read distance of up to 6m for mmWave backscatter signals using the CSI. (2) In an indoor environment with other reflectors around, we demonstrate that it is still possible to distinguish between open and short states of mmWave backscatter. (3) We find that it is possible to scan all sectors (as in 802.11ad beacons or beamforming) to determine the sectors in which an mmID tag is located and backscatter signal is received. (4) When there are mmWave backscatter tags deployed in the environment, beamscanning can be used to periodically determine their reachability. We show that this information can be readily translated to surrounding blockages and can be leveraged by the APs to perform intelligent beamforming to clients through a constrained search. We discuss how the mmWave backscatter can enable a new research direction realizing a truly integrated framework for mmWave networking, sensing and applications.

2 BACKGROUND AND RELATED WORK
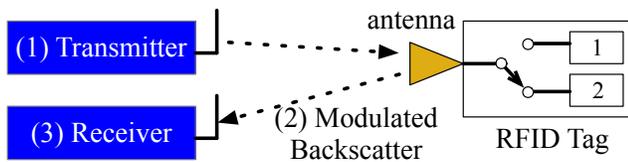
2.1 Backscatter background

Figure 1: A simplified view of a bistatic backscatter system shows that the RFID tag can modulate the backscatter signal by switching two different impedances (circuit1 & circuit2).

A bistatic backscatter system consists of a transmitter, receiver, and a backscattering tag. Here, as shown in the Fig. 1, (1) the transmitter sends a signal to the backscatter tag which reflects the incoming signal. At the same time, the tag can employ various modulation

techniques (amplitude, phase, and/or frequency modulation [9, 31]) on the backscattered signal. (2) Fig. 1 shows a modulated backscatter that uses amplitude modulation by switching RF loads with different impedance, resulting in two modulation states of high and low power radiated backscatter signal. (3) The receiver demodulates the backscattered signal to retrieve the tag information.
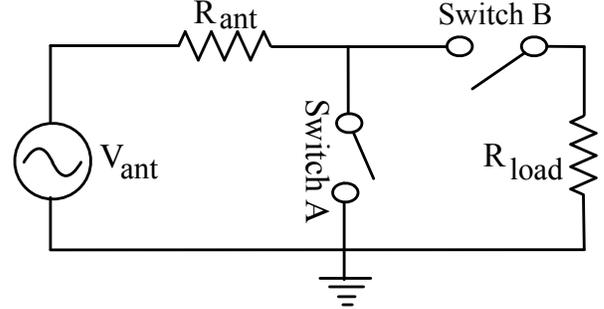

Figure 2: It shows a simplified circuit of a backscatter tag using tag antenna and switch circuit. The tag antenna is represented as its Thevenin equivalent where V_{ant} and R_{ant} indicate the induced voltage and antenna impedance, respectively. The switch circuit controls the switches A and B to connect the ground or chip impedance R_{load}.

Switch States	Switch A	Switch B	Radiated Power
Open	X	X	0
Short	O	X	$\frac{V_{ant}}{R_{ant}}$
Matched load	X	O	$\frac{V_{ant}}{4 \times R_{ant}}$

Table 1: Different backscatter states and radiated power (X - switch open, O - switch closed). If switches A and B are not connected (Open state), no energy is released, while all received power is re-radiated again by connecting only switch A (Short state).

To generate the amplitude modulation states, a tag can have different types of load: open, short and matched load circuit. A simplified circuit of a backscatter tag is shown in Fig. 2. Here the antenna is represented as a voltage source V_{ant} and R_{ant} arising from the signal transmitted by the transmitter. R_{ant} is a resistance of the antenna and R_{load} is the resistance of the IC chip connected to the antenna. In the case of an open circuit, paths to both ground and IC chip are blocked, resulting in no current in the antenna and no power in backscattered signal (refer Table 1). In the case of a short circuit, the current flows directly to the ground, so the largest power in the radiated signal is generated while the current is flowing over the R_{ant}. Finally, in the case of matched loads, due to the impedance matching between an antenna and IC chip (same R_{ant} and R_{load}), half of the energy flows into the IC. The total current flowing can be calculated as $\frac{V_{ant}}{R_{ant}+R_{load}}$. The three states can be generalized through a range of impedance values, creating a higher-order amplitude modulation.

2.2 Related work

RFID backscatter using commodity radios has been investigated extensively at 2.4 GHz [16, 33] (refer [31] for a survey) and has been leveraged for localization [2, 19] and cross-technology communication [14, 32].

In terms of mmWave, an mmID system was first introduced in [25] where authors designed a tag and analyzed its performance theoretically as well as through experiments. The authors showed that an mmID with 0 dBi antenna gain had a read distance of only 0.5m. Since then the research on mmID has been primarily in two directions - design of the tag and novel applications. First, [6, 13, 18, 23, 24] have focused on the design of the mmWave tag and a customized reader. Authors in [13] designed a tag with high antenna gain (18.6 dBi) & miniaturized antenna size ($26.8 \times 32.5mm$) while [6] presented a design which achieves 10dB modulation gain at 58.75 GHz. Similarly, [23] presented a fully integrated RFID tag with Intel 90 nm CMOS. However, these mmWave tag designs are not publicly available and more importantly, they are shown to only operate with custom-made readers.

Second, some recent research papers have shown how mmWave backscatter can enable novel sensing applications due to the advantages of mmID (directionality and large bandwidth). Authors in [17] demonstrated presence detection and soil moisture sensing using mmWave backscatter. They also showed a proof-of-concept wideband OFDM backscatter system. Authors in [11] developed a mmWave tag localization system which can use a single reader to localize the tag to a few centimeter accuracies up to 6.7m distance. These papers showcase the potential of mmWave backscatter, however, they leverage a custom and dedicated reader with high-gain horn antennas. On the other hand, our focus in this work is to demonstrate how commodity 802.11ad radios can be used as mmWave backscatter readers.

In other similar work, authors in [1] develop a mmWave signal relay that can steer the reflected signal in the intended direction and provide connectivity in the presence of blockages. Similarly, smart reflect-arrays are presented in [28] where mmWave signals can be reflected and steered towards the receiver. In comparison, mmWave backscatter is more flexible and can provide functionality beyond just the relaying by modulating the reflected signal. Also, the reflect-array system is developed using non-COTS devices, while our work focuses on COTS 802.11ad devices as the backscatter reader.

3 IMPLEMENTATION AND EXPERIMENT SETUP

In this section, we describe our testbed setup and implementation of mmWave backscatter system.

3.1 802.11ad mmID Reader Devices

Our objective is to demonstrate the use of the COTS 802.11ad device as an interrogator/reader of mmWave backscattering signal without any hardware or protocol modifications. We choose Airfide 802.11ad access points [3] for this purpose. The devices use Qualcomm QCA9500 IEEE 802.11ad Wi-Fi chip with QCA6335 baseband chip and QCA6310 for RF front-end. The APs are equipped with 8 phased arrays where each array has 32 antenna elements (shown in Fig. 3). With these high-gain antenna arrays, the devices can

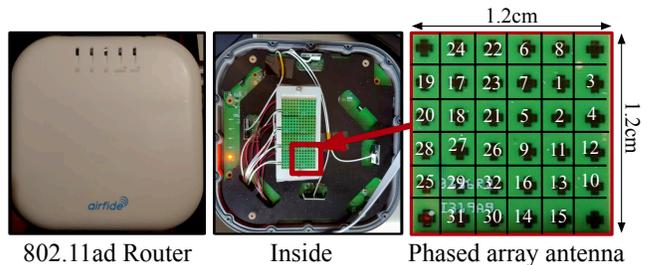802.11ad Router   Inside   Phased array antenna

Figure 3: The 802.11ad platform used as our mmWave backscatter reader. The numbers on the phased array antenna (right-most figure) represent the index of 32 antenna elements.

provide up to 40 dBm of EIRP (maximum allowable as per FCC [7]). The 8 antenna arrays can be arranged in various configurations (1×1, 1×4, 2×2, and 2×4). In our work, we only leverage a single antenna array (1×1) to demonstrate the feasibility of detecting the backscatter even at a lower EIRP of 35 dBm [3].

CSI extraction. The Airfide platform is supported by OpenWrt and adopts the open-source Wil6210 802.11ad kernel driver. The platform does not provide the CSI measurements that can be readily used for our purpose. Recent work [4] has extracted the CSI measurements from the TP-Link Talon AD7200 IEEE 802.11ad AP through driver modifications. However, the Talon devices use a different antenna array [21] which has a non-uniform element arrangement [27] and lower antenna gain. Instead, we modify the Wil6210 driver on Airfide to add a vendor-specific command that can extract the CSI from the firmware. When the command is issued from the user-space, the driver sends the command to the RF controller. The CSI report buffer is 128 bytes in size which include 64 bytes of phase (2 bytes for each of the 32 elements) and 64 bytes for amplitude (2 bytes each for 32 elements) as shown in Fig. 4. The reported phase value ranges from 0 to 1023 while the amplitude value ranges from 0 to 178.

In the current implementation, the CSI collection requires initiating the beam refinement process (BRP). However, this is a driver limitation and can be extended to achieving the CSI measurement for every 802.11ad frame with channel estimation training fields. In 802.11ay, the beacon frames include the training fields similar to BRP [8] which can enable more frequent CSI measurements.

Sector selection. The Airfide transmitter uses the default codebook providing 50 sectors with different beam patterns. We set the Airfide receiver to use the quasi-omni beam sector. By default, the BRP process only reports the CSI for the best transmit sector found after the search process. To achieve CSI for all sectors during the BRP, we develop additional driver modifications that can (1) set a desired transmit (or receive) sector or (2) activate only a subset of transmit (or receive) sectors to search from. This way, we are able to achieve phase and amplitude for all antenna elements in all transmit sectors.
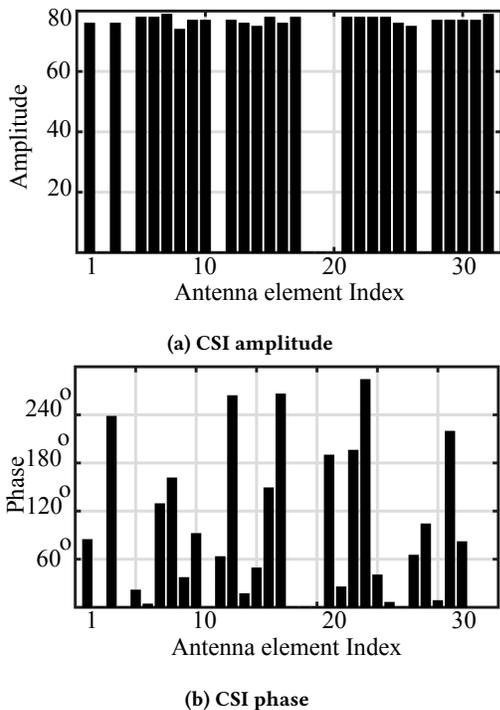
(a) CSI amplitude

(b) CSI phase

Figure 4: The CSI report contains amplitude and phase of 32 antenna elements (in 1×1 antenna array configuration). The figure shows the CSI measurement between an AP and a client (both Airfide) when placed at $1m$ distance facing each other. Some of the antenna elements do not show amplitude depending on the chosen antenna sector's weight vector.

3.2 mmWave Backscattering Tag

The development of a fast-switching semi-passive mmWave backscatter tag using a patch antenna is part of our ongoing work. In this work, we use a 60 GHz horn antenna and manually switch it between open-circuit and short-circuit to generate two amplitude modulation stages of a tag as described in Section 2.1. This implementation of the tag does not have an IC (shown in Fig. 5), however, it works well in demonstrating that these two stages of backscatter modulation (albeit switched manually) can be detected through CSI on the 802.11ad reader. Testing mmWave tags in this way is also important for comparison, as it provides the optimal backscattering performance [12].

The short-circuit (SC) and open-circuit (OC) using the horn antenna are achieved through a calibration short with and without the shim, respectively. The matched-load (ML) offers an impedance match for the horn antenna. This is shown in Fig. 5. The antenna short attached to the WR-15 waveguide creates a short-circuited antenna, providing the smallest possible load and highest possible backscattered signal. Another stage of modulation, i.e., the open-circuit antenna, can be realized by adding a quarter-wave shim which transforms the waveguide short into an open through quarter-wave impedance transformation [5]. This results in the highest and lowest possible backscattered signal. We use SWO-15-F1 open shim and short [10] attached to the PE9881-24 horn

Figure 5: Horn antenna converted to the short and open-circuited antenna using a calibration short with and without the quarter-wavelength shim, respectively. The matched load offers an impedance match for the horn antenna.

antenna [22]. The open shim has a thickness of 0.061 inch which adds an additional $\frac{\lambda}{4}$ line distance to the short as shown in Fig. 5. Since the frequency band range of the horn antenna is from 50 GHz to 75 GHz, the center frequency is 62.5 GHz. The 0.061 inch quarter wavelength is computed using

$$\lambda_{\text{quarter}} = \frac{\frac{\lambda_{\text{center}}}{\sqrt{1 - (\frac{\lambda_{\text{center}}}{\lambda_{\text{cut-off}}})^2}}}{4} \tag{1}$$

where the wavelength of cut-off frequency $f_{\text{cut-off}}$ (39.9 GHz) and center frequency f_{center} (62.5 GHz) are 0.29 inch and 0.19 inch, respectively. Because the quarter wavelength offers the perfect open at the frequency of 62.5 GHz, we run all our experiments at 802.11ad Channel 3 which has a center frequency at 62.64 GHz.

4 MMWAVE BACKSCATTER CHARACTERIZATION

Using the 802.11ad devices and mmWave backscatter tag implementation, we now discuss our empirical characterization of backscattering mmWave signal at different read distances and angles in indoor as well as outdoor environment. From extensive experiments, we find that the tag response indicates the tag direction and reachability information. We then discuss how tag's reachability (blocked or not) from the AP can augment the beamforming process in 802.11ad WLANs.

Read distance. Fig. 6 shows our experiment setup. Two Airfide devices (one acting as an AP and the other as a station) are placed next to each other to imitate a bistatic reader. The two devices are separated by mmWave signal absorbers to reduce their direct communication due to the Rx quasi-omni pattern. The direct communication can be significantly reduced using Rx beamforming. We first perform these experiments outdoors to minimize the impact of multi-path in our observations. The tag is placed in front of the reader at the broadside angle of $0°$. We analyze the Airfide codebook and find that sector ID 63 shows the highest gain at the same
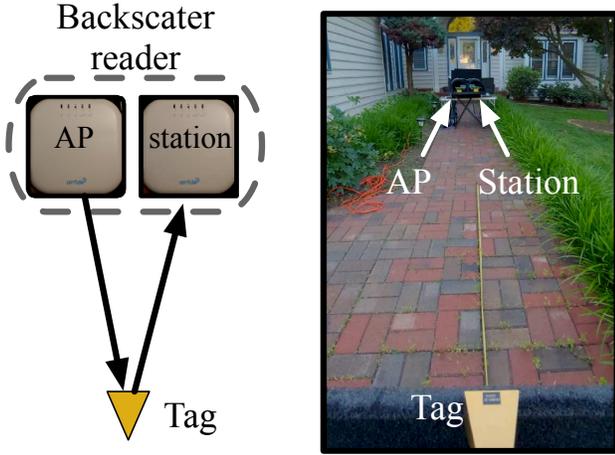
Figure 6: Our outdoor experiment setup for distance measurements. The AP and station form the backscatter reader as the left-side figure.
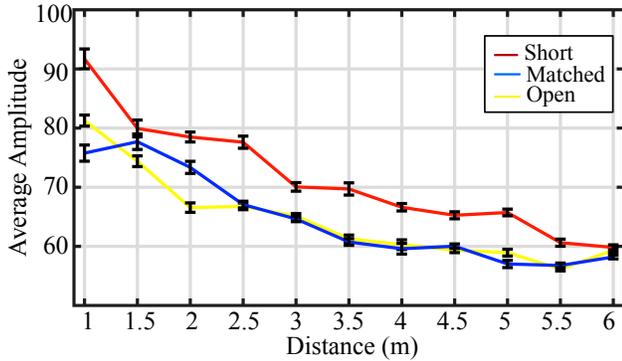

Figure 7: The average amplitude of 32 antenna elements in short, open, and matched load cases of mmWave backscatter.

angle. We set the AP's transmit sector to 63 and set the station's receive sector to quasi-omni.

Fig. 7 shows the average amplitude for each of the 32 elements on the receiver when the signal reflects from the mmID tag as we vary the distance and switch the tag states between open-circuit, short-circuit and matched load at each distance. Figs. 8(a) and (b) show the amplitude difference between open and short and between matched load and short, respectively. We repeat the experiments for 75 times at each position to ensure the reproducibility. As expected, the amplitude decreases with increasing distance. However, we observe that both open/short and matched load/short amplitude have a clearly discernible difference up to 6m, proving the feasibility of 802.11ad CSI based mmWave backscatter reader. Prior work [11] has shown the mmID read distance of up to 6.7m using a custom, a non-COTS reader that is equipped with a high-gain horn antenna. Here, we verify that we can achieve a comparable read range using CSI on 802.11ad COTS devices. We observe that amplitude observed for each element is noticeably different due to the shorter wavelength
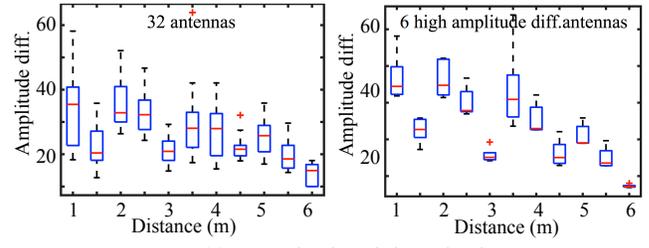
(a) open-circuit and short-circuit
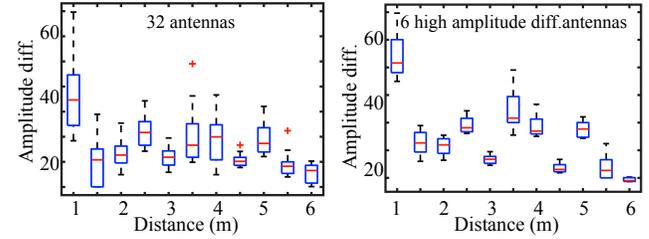
(b) matched load and short-circuit

Figure 8: Amplitude difference between open, short, and matched load cases of mmWave backscatter. The figures on the left-side show the amplitude difference of all 32 antenna elements. The figures on the right-side shows the top 20% antenna elements with high amplitude difference.

of mmWave. Our experiments show that these amplitude values are highly sensitive to the alignment between the reader's antenna arrays and the tag antenna.

Findings: We find that 802.11ad COTS devices can be leveraged as mmWave backscatter readers using the CSI measurements. They can provide a read distance of up to 6m, making it possible to enable a range of networking and sensing applications.
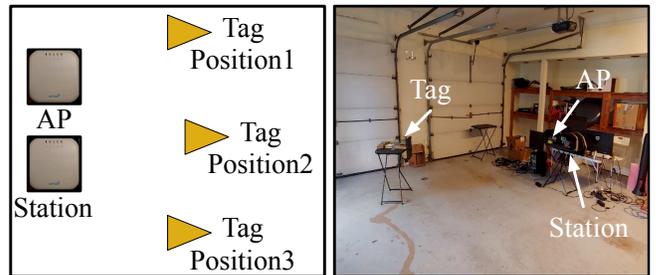

Figure 9: Our indoor experiment setup with a tag at different positions and angles relative to the reader.

Different locations and beam sectors. We now characterize the mmWave backscatter in indoor environments with rich multi-path. We place the tag at 3 different positions (broadside $-45°$, $0°$, and $+45°$) in a $6m \times 7m$ garage[1]. Due to the small size of room and 35dBm high Tx power, our test environment has significant multi-path. The experiment setup is shown in Fig. 9. The Airfide transmitter scans all 50 sectors one by one (similar to sector sweeping in 802.11ad) and records their CSI. The scanning is repeated 25 times with each scanning and CSI collection instance lasting for 1-2 minutes.

---

[1]Due to the Covid-19 pandemic, the experiments could not be performed in larger university rooms or more realistic office settings.
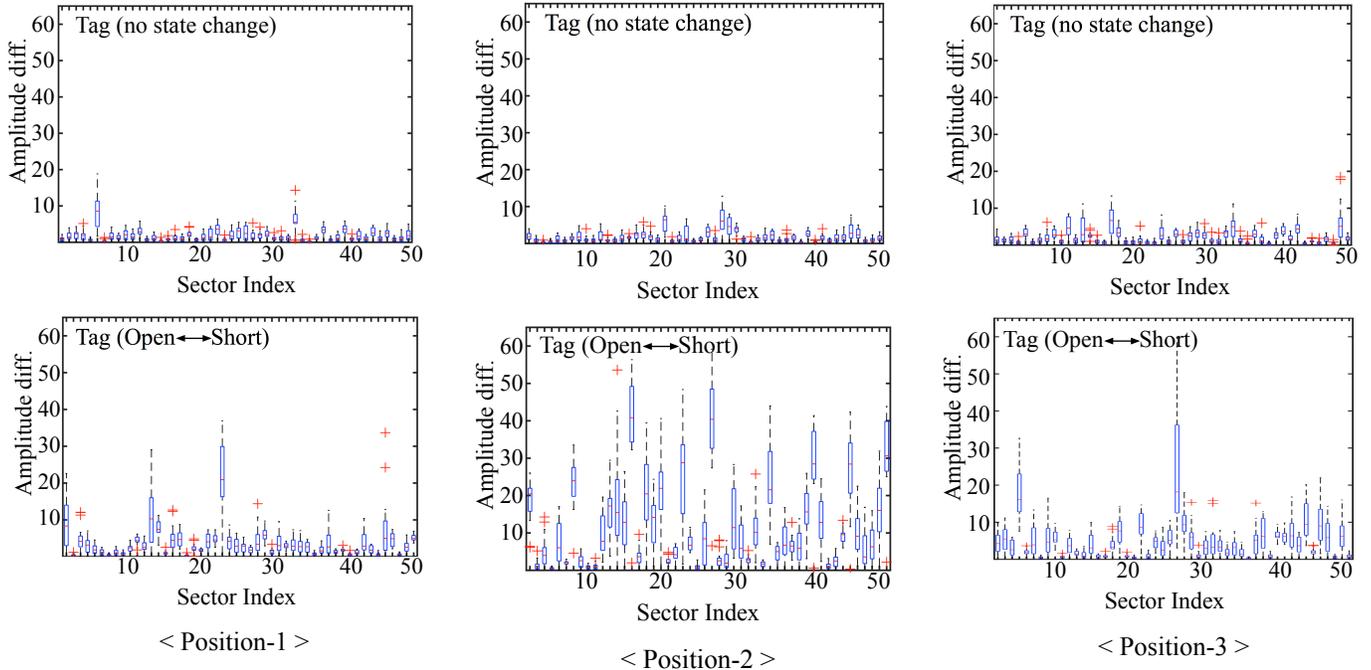
Figure 10: Amplitude difference observed in different sectors at three positions (for three mmWave backscatter cases: tag without open or short, open circuit and short circuit)

Fig. 10 shows the difference between open and short amplitude for all 50 sectors at each of the three tag positions. For comparison, we also include the amplitude when the antenna tag is placed at the position without switching between open or short-circuited. This is to confirm that the amplitude difference observed is indeed due to open-short state change and not the indoor multi-path. We make multiple observations. First, we find that even in the indoor environment with non-negligible multi-path, it is possible to clearly distinguish the open and short-circuit amplitude. This shows that CSI-based detection of mmWave backscatter is feasible indoors as well. Second, as expected, the position of the mmID tag dictates the sectors in which the tag open-short difference is more prominent. For example, Sector 25 shows an amplitude difference of 59.2 when the tag is placed at Position-2 and switched between open and short, whereas the difference is only 5.16 when the tag is placed there without open or short.

Since many sectors have gained in broadside 0°, the center position of the tag registers clear open-short amplitude difference in all of them. Overall, we find that it is possible to scan all sectors (similar to the beamforming process) and identify the sectors and direction in which the tag is located. Here, only sectors with higher gain in the tag direction will have a clear amplitude difference. Therefore, the beam pattern direction may represent the tag direction. For example, in case of Position-1, if we consider to set the threshold of CSI amplitude difference as 20, a tag at the Position-1 responds to sector IDs {0,12,22}, while in case of Position-3, it responds to sector IDs {3,26,43}. This approximate localization of the tag can be extended to a more accurate location through additional information such as antenna sector patterns and time of flight.

Findings: CSI-based detection of mmWave backscatter on 802.11ad devices is also feasible in multi-path rich indoor environments with other mmWave reflectors. Beam scanning can be used to determine the sectors and approximate directions in which the tag is located. This information can be useful in various WLAN design problems, such as blockage detection, localization, and efficient beamforming as we demonstrate in the next section.

5 MMWAVE BACKSCATTER APPLICATION IN 802.11AD WLAN

Detecting tag reachability using CSI. We now show that using CSI we can not only detect the existence of a tag but also if there is a blockage between the reader and the tag. To verify this, we place a tag at 2.5m distance from the reader AP and measure the tag response with and without a human blockage as the tag switches its state between open and short. The experiment is repeated multiple times (up to 150 measurements) to verify reproducibility. A representative scenario is shown in Fig. 11. It can be observed that before a blockage occurs, the CSI measurements show an average amplitude difference of 26.3, while the difference drops to 3.4 in the presence of the blockage. This shows that APs can monitor the tag response over time through the CSI measurements. The CSI pattern can be used to detect the presence of a blockage.

Reducing the beamforming overhead. We now consider how mmWave backscatter detected through 802.11ad devices can be helpful in reducing the beamforming overhead in a 60 GHz WLAN. As mentioned before, beacons sent out in all sectors or beam scanning can be used to determine the sectors in which a tag's response can be received. The AP can repeatedly probe these sectors to see
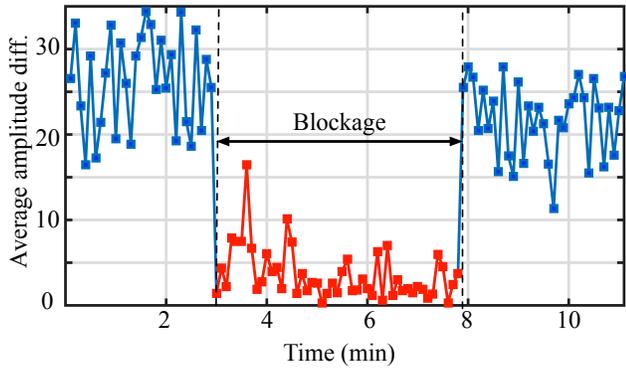
Figure 11: The CSI amplitude difference substantially reduces when the tag is blocked from the reader by the human body.
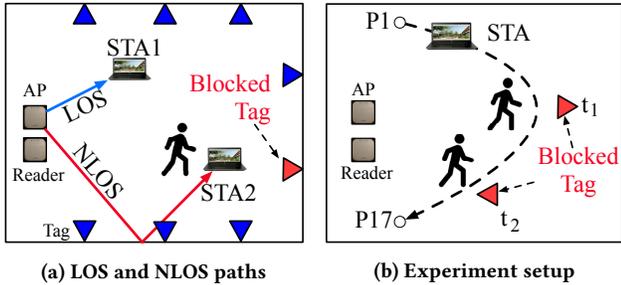

(a) LOS and NLOS paths   **(b) Experiment setup**

Figure 12: Reducing beamforming overhead through tag reachability detection.
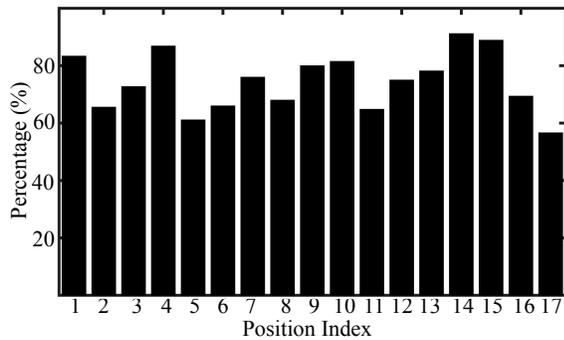

Figure 13: The probability that (or percentage of instances where) the best sector (highest SNR) found through 802.11ad's exhaustive search belongs to the subset of sectors that are not blocked based on the reachability of backscatter tags.

if the tag is reachable or blocked. Through periodic beacons, the AP can probe all tags deployed in the environment to determine their reachability status and infer the current blockages in its surroundings. This information (sectors where a tag responds and the tag's current status i.e., reachable or blocked) can be then used for reducing the beamsearching overhead for the clients associated with the AP.

Let us consider a scenario where N low-power, low-cost mmID tags (referred by set T_N) are deployed in a room. Let S be the set

of all transmit sectors at the AP and $S^{t_i} \subset S$ be the subset of AP sectors where tag t_i responds (the discernible difference between modulation states). We assume that second-order reflections (from tag to wall to reader) are not feasible due to already low radiated backscatter power. Hence, for each sector $s_j^{t_i} \in S^{t_i}$, the tag t_i responds directly over the LoS path to the AP. Let T_B and T_R be the subset of tags that are currently either blocked or reachable from the AP respectively. Through the periodic beamscanning, the AP can determine the S_B which is the union of sectors associated with tags in T_B. The remaining sectors form the set $S_R = S - S_B$. As shown in Fig. 12a, we claim that when the AP performs transmit beamsearching with STA1, the resultant sector belongs S_R with a high probability. This is also true for a station (STA2) which is closer to a blocked tag where the best transmit sector from the AP uses a reflected path. AP can perform a restricted beamsearching (only over S_R sectors instead of all S) to reduce the searching overhead. Detecting the reachability of the tags does not incur any additional overhead as it can be accomplished just using the default beaconing process. Additionally, such a restricted beamsearching does not require prior knowledge about the antenna patterns.

To verify the above claim, we perform an evaluation using the indoor scenario discussed before. We place two tags at different positions as shown in Fig. 12b. We first find their set of associated sectors S^{t_1} and S^{t_2}. Two blockages are then created to block the tags from the AP, hence, forming $S_B = S^{t_1} \cup S^{t_2}$. A station (connectable to the AP) is placed at 17 different positions (P_1 to P_{17}). As discussed above, all sectors excluding the sectors associated with the blocked tags (i.e., S_R) are searched from AP to the STA at each of the 17 positions. We have presented a simplified scenario here where we assume that whenever a tag is blocked, the blockage also occurs between the AP and the station. This is also true if the tag is attached to the client device (e.g., on the phone or laptop). In a more generic scenario, this assumption can be relaxed by using multiple densely deployed tags and/or readers. The beamsearching is repeated 50 times at each position. Fig. 13 shows the probability that the best sector found after exhaustive beamsearching belonged to S_R. We find that 74.4% of the time the best sector is within the set of sectors excluding the sectors associated with the tags that are currently blocked. Even for Positions P_9 and P_{13} where the tag and STA both are blocked, the AP uses a reflected sector which is found to be present in S_R more than 80% of the instances. As the tag deployment density increases, such restricted beamforming can yield significant savings in terms of beamsearching overhead (26.4% fewer beams searched compared to exhaustive search in our experiment with only two tags). Additionally, a dense deployment of tags and multiple APs/readers can be exploited to obtain more detailed information about blockages in the surrounding. Similarly, the tags can be attached to WLAN stations making it possible to track their mobility and reduce the beamsearching overhead. Overall, the integration of mmWave backscatter in 60 GHz WLANs can improve their efficiency and agility to blockages and mobility, paving the way for an integrated mmWave networking, sensing and application framework.

6 CONCLUSION AND DISCUSSION

In this paper, we presented an empirical evaluation of mmWave backscatter using 802.11ad 60 GHz COTS radios. Our experiments showed that COTS devices can provide a read distance of up to $6m$ at various angles and locations. We also demonstrated an application of mmWave backscatter where the tags are used to determine the blockages and perform constrained beamsearching to reduce the searching overhead. Our presented evaluation is the first step towards realizing a fully functional mmWave COTS backscatter system. Our presented work does not consider receive beamforming on the reader side as well as phase modulation on the backscatter tag side. Both of these can improve the read distance and provide a more robust detection of mmWave backscatter. Also, our work does not consider a MAC protocol for backscatter (similar to RFID Gen2) essential in a dense deployment of tags. Our experiment is based on the bi-static reader scenario due to the horn antenna beamwidth, but according to the prototype development, we plan to further explore other scenarios with a wider beamwidth antenna on the tag. We plan to investigate these challenges in our ongoing mmWave backscatter prototype development.

REFERENCES

[1] Omid Abari, Dinesh Bharadia, Austin Duffield, and Dina Katabi. 2017. Enabling high-quality untethered virtual reality. In *14th {USENIX} Symposium on Networked Systems Design and Implementation ({NSDI} 17)*. 531–544.

[2] Ajibayo O Adeyeye, Jimmy Hester, and Manos M Tentzeris. 2019. Miniaturized Millimeter Wave RFID Tag for Spatial Identification and Localization in Internet of Things Applications. In *2019 49th European Microwave Conference (EuMC)*. IEEE, 105–108.

[3] Airfide 2019. AFN2200. https://airfidenet.com/.

[4] Hany Assasa. 2019. *Robust and reliable millimeter wave wireless networks*. Ph.D. Dissertation. Universidad Carlos III de Madrid.

[5] G. Bonaguide and N. Jarvis. 2019. *The VNA Applications Handbook*. Artech House. https://books.google.com/books?id=PvGZxgEACAAJ

[6] Horacio I Cantú, David RS Cumming, and Timothy D Drysdale. 2011. Active V-band modulated backscatter tag. *Microwave and Optical Technology Letters* 53, 7 (2011), 1613–1615.

[7] Federal Communications Commission et al. 2013. FCC 13-112: In the Matter of Revision of Part 15 of the Commission's Rules Regarding Operation in the 57-64 GHz Band. *ET Docket No. 07* 113 (2013).

[8] Claudio RCM Da Silva, Jonathan Kosloff, Cheng Chen, Artyom Lomayev, and Carlos Cordeiro. 2018. Beamforming training for IEEE 802.11 ay millimeter wave systems. In *2018 Information Theory and Applications Workshop (ITA)*. IEEE, 1–9.

[9] Daniel M Dobkin. 2012. *The rf in RFID: uhf RFID in practice*. Newnes.

[10] Eravant 2019. WR-15 WAVEGUIDE OPEN. https://www.eravant.com/.

[11] Francesco Guidi, Nicoló Decarli, Davide Dardari, Francesco Mani, and Raffaele D'Errico. 2018. Millimeter-wave beamsteering for passive RFID tag localization. *IEEE Journal of Radio Frequency Identification* 2, 1 (2018), 9–14.

[12] David Hotte, Romain Siragusa, Yvan Duroc, and Smail Tedjini. 2015. Radar cross-section measurement in millimetre-wave for passive millimetre-wave identification tags. *IET Microwaves, Antennas & Propagation* 9, 15 (2015), 1733–1739.

[13] David Hotte, Romain Siragusa, Yvan Duroc, and Smail Tedjini. 2017. Design of a planar passive MMID tag antenna. *IET Microwaves, Antennas & Propagation* 11, 12 (2017), 1770–1775.

[14] Vikram Iyer, Vamsi Talla, Bryce Kellogg, Shyamnath Gollakota, and Joshua Smith. 2016. Inter-technology backscatter: Towards internet connectivity for implanted devices. In *Proceedings of the 2016 ACM SIGCOMM Conference*. 356–369.

[15] Nemai C Karmakar et al. 2013. Chipless RFID tag localization. *IEEE transactions on Microwave Theory and Techniques* 61, 11 (2013), 4008–4017.

[16] Bryce Kellogg, Vamsi Talla, Joshua R Smith, and Shyamnath Gollakot. 2017. PASSIVE WI-FI: Bringing low power to Wi-Fi transmissions. *GetMobile: Mobile Computing and Communications* 20, 3, 38–41.

[17] John Kimionis, Apostolos Georgiadis, and Manos M Tentzeris. 2017. Millimeter-wave backscatter: A quantum leap for gigabit communication, RF sensing, and wearables. In *2017 IEEE MTT-S International Microwave Symposium (IMS)*. IEEE, 812–815.

[18] Tero Kiuru, Pekka Pursula, Joose Rajamäki, and Tauno Vähä-Heikkilä. 2013. A 60-GHz semipassive MMID transponder for backscattering communications. In *2013 IEEE MTT-S International Microwave Symposium Digest (MTT)*. IEEE, 1–3.

[19] Manikanta Kotaru, Pengyu Zhang, and Sachin Katti. 2017. Localizing low-power backscatter tags using commodity wifi. In *Proceedings of the 13th International Conference on emerging Networking EXperiments and Technologies*. 251–262.

[20] Lionel M Ni, Yunhao Liu, Yiu Cho Lau, and Abhishek P Patil. 2003. LANDMARC: indoor location sensing using active RFID. In *Proceedings of the First IEEE International Conference on Pervasive Computing and Communications, 2003.(PerCom 2003)*. IEEE, 407–415.

[21] Joan Palacios, Daniel Steinmetzer, Adrian Loch, Matthias Hollick, and Joerg Widmer. 2018. Adaptive codebook optimization for beam training on off-the-shelf ieee 802.11 ad devices. In *Proceedings of the 24th Annual International Conference on Mobile Computing and Networking*. 241–255.

[22] Pasternack 2019. WR-15 Waveguide Standard Gain Horn Antenna. https://www.pasternack.com/.

[23] Stefano Pellerano, Javier Alvarado, and Yorgos Palaskas. 2010. A mm-wave power-harvesting RFID tag in 90 nm CMOS. *IEEE Journal of Solid-State Circuits* 45, 8 (2010), 1627–1637.

[24] P. Pursula, F. Donzelli, and H. Seppa. 2011. Passive RFID at Millimeter Waves. *IEEE Transactions on Microwave Theory and Techniques* 59, 8 (2011), 2151–2157.

[25] Pekka Pursula, Tauno Vaha-Heikkila, Alexandru Muller, Dan Neculoiu, George Konstantinidis, Aarne Oja, and Jussi Tuovinen. 2008. Millimeter-wave identification—A new short-range radio system for low-power high data-rate applications. *IEEE Transactions on Microwave theory and techniques* 56, 10, 2221–2228.

[26] Longfei Shangguan and Kyle Jamieson. 2016. The design and implementation of a mobile RFID tag sorting robot. In *Proceedings of the 14th annual international conference on mobile systems, applications, and services*. 31–42.

[27] Daniel Steinmetzer, Daniel Wegemer, Matthias Schulz, Joerg Widmer, and Matthias Hollick. 2017. Compressive millimeter-wave sector selection in off-the-shelf ieee 802.11 ad devices. In *CoNEXT 17*. 414–425.

[28] Xin Tan, Zhi Sun, Dimitrios Koutsonikolas, and Josep M Jornet. 2018. Enabling indoor mobile millimeter-wave networks based on smart reflect-arrays. In *IEEE INFOCOM 2018-IEEE Conference on Computer Communications*. IEEE, 270–278.

[29] Jue Wang and Dina Katabi. 2013. Dude, where's my card? RFID positioning that works with multipath and non-line of sight. In *Proceedings of the ACM SIGCOMM 2013 conference on SIGCOMM*. 51–62.

[30] Ke Wu, Pascal Burasa, Tarek Djerafi, and Nicolas Constantin. 2016. Millimeter-wave identification for future sensing, tracking, positioning and communicating systems. In *2016 Global Symposium on Millimeter Waves (GSMM) & ESA Workshop on Millimetre-Wave Technology and Applications*. IEEE, 1–4.

[31] Chenren Xu, Lei Yang, and Pengyu Zhang. 2018. Practical backscatter communication systems for battery-free Internet of Things: A tutorial and survey of recent research. *IEEE Signal Processing Magazine* 35, 5 (2018), 16–27.

[32] Chenren Xu, Lei Yang, and Pengyu Zhang. 2018. Practical backscatter communication systems for battery-free Internet of Things: A tutorial and survey of recent research. *IEEE Signal Processing Magazine* 35, 5 (2018), 16–27.

[33] Pengyu Zhang, Dinesh Bharadia, Kiran Joshi, and Sachin Katti. 2016. Hitchhike: Practical backscatter using commodity wifi. In *Proceedings of the 14th ACM Conference on Embedded Network Sensor Systems CD-ROM*. 259–271.